



## Quantum coherence enhancement by the chirality-induced spin selectivity effect in the radical-pair mechanism

Yash Tiwari  and Vishvendra Singh Poonia \*

*Department of Electronics and Communication, Indian Institute of Technology, Roorkee, Uttarakhand - 247667, India*

 (Received 8 December 2022; revised 19 March 2023; accepted 27 April 2023; published 15 May 2023)

This work investigates the effect of chirality-induced spin selectivity (CISS) on quantum coherence in the radical-pair (RP) mechanism of avian magnetoreception. Additionally, we examine the correlation of global and local coherence measures with the yield of the signaling state in the RP model. We find that both relative entropy of global coherence and local coherence in the radical pair increase with CISS. However, only global coherence shows a strong correlation with the signaling state yield and thus indicates a plausible utilitarian role for the avian compass. We also analyze the interplay of dipolar and exchange interaction with the CISS and their effect on the coherence of the radical-pair spin. Further, we analyze the effect of environmental decoherence along with CISS. We conclude that a high CISS results in a high correlation of global coherence with signaling state yield. We propose that CISS might play an important role in developing quantum technologies by sustaining coherence in radical-pair-like quantum systems.

DOI: [10.1103/PhysRevA.107.052406](https://doi.org/10.1103/PhysRevA.107.052406)

### I. INTRODUCTION

Quantum coherence is a resource for quantum technologies. But its existence in biological systems in ambient conditions and its functional utility in biophysical processes have been extremely intriguing and debatable subjects [1,2]. Avian magnetoreception is one such biological process wherein the radical-pair spin dynamics have been investigated from several aspects, wherein part of the focus has been to understand the role and utility of quantum coherence in it [3–10]. Interestingly, a unitary-dilation-based quantum algorithm approach has been used recently to study the radical-pair spin dynamics, giving a new tool to examine the avian compass [11]. The radical-pair mechanism is based on a spin-sensitive chemical reaction that is mediated by the cryptochrome protein molecule [12,13]. Owing to the chirality of protein molecules, the chirality-induced spin selectivity (CISS) effect might play an important role in the electron transport part of the reaction. The origin of CISS is attributed to the spin-orbit interaction and the electrostatic potential provided by the chiral molecules [14–18]. It was shown by Fay *et al.* [19] that chirality in conjunction with spin-orbit interaction in electron transfer reactions generates coherence locally. It was done for the electron spin-echo experiment. It was also shown in Ref. [20] that the prerequisite for forming a radical pair for avian magnetoreception is the transfer of electrons. Owing to growing evidence of the role of chirality-induced spin selectivity in electron transfer and charge reorganization mechanisms [14,15,21–25], we investigate the plausible ramifications of CISS in the radical-pair mechanism. To probe the relationship between CISS and quantum coherence, we quantify the coherence based on standard quantifiers. These are

based on the offdiagonal (coherence) elements of the density matrix of the quantum state [26–30]. It has been suggested in Refs. [3,31] that global coherence rather than local or electronic coherence might enhance the compass sensitivity. Therefore, we correlate the yield of the spin-selective chemical reaction with the coherence measures in a chiral medium for the avian magnetoreception.

In this work, we make use of relative entropy of coherence [26] and total coherence [5] measures as coherence quantifiers to answer the following questions: (i) how does the CISS affect the local and global coherence measures in the radical-pair mechanism, (ii) how do dipolar and exchange interactions in conjunction with CISS affect the total local and global coherence measures, (iii) how does the environmental decoherence affect the multinuclei radical-pair mechanism, and, more importantly, (iv) is the quantum coherence related to the yield of the radical-pair mechanism? If yes, in what form? We have considered cases up to four nuclei each on flavin adenine dinucleotide  $\text{FAD}^{\cdot-}$  and tryptophan  $\text{TrpH}^+$  radicals. The FAD acts as an electron acceptor, whereas TrpH acts as an electron donor. The hyperfine interaction values of these nuclei have been taken from Ref. [12] and are given in Appendix A.

The manuscript has been organized as follows: Section II discusses the methodology followed for the analysis. Section III discusses the results, wherein Sec. III A discusses the effect of CISS on quantum coherence measures and Sec. III B explores the impact of electron-electron interactions on system sensitivity along with its interplay with CISS. Section III C illustrates an increase of coherence due to CISS at various rate constants. Section IV demonstrates the effect of environmental decoherence on the system. Section V examines the correlation of the quantum coherence with the reaction yield of the radical-pair model. We have used QUTIP [32] for our calculations.

\*vishvendra@ece.iitr.ac.in

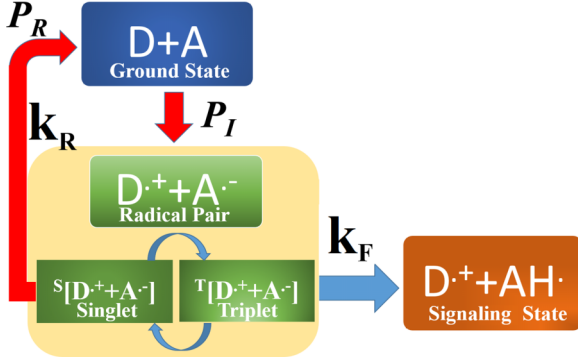


FIG. 1. The schematic for the CISS-assisted radical-pair mechanism, where  $D$  denotes the donor molecule,  $A$  represents the acceptor molecule,  $D^+$  is the donor radical,  $A^-$  is the acceptor radical,  $k_F$  is the protonation rate constant to the signaling state, and  $k_R$  is the recombination rate constant to the ground state. The red arrows represent the role of CISS in the reaction pathways.

## II. METHODOLOGY

In the radical-pair model of the avian magnetoreception, an electron is photoexcited in the acceptor molecule, creating a vacancy in the ground state. Another electron from a neighboring donor molecule travels in the chiral medium to fill this vacancy. It results in the formation of a radical pair. The spin operator of the electron on the donor molecule is  $\hat{S}_D$  and on the acceptor molecule is  $\hat{S}_A$  [20,33]. Therefore, the spin state of the above-formed radical pair is governed by the following Hamiltonian [20,34,35]:

$$\hat{H} = \omega(\hat{S}_A + \hat{S}_D) + \sum_{i \in D, A} \sum_k \hat{S}_i A_{ik} \hat{I}_{ik} - J(2\hat{S}_A \hat{S}_D + 0.5) + \hat{S}_A D \hat{S}_B, \quad (1)$$

where  $\omega = g\mu_B \bar{B}$ ,  $\bar{B} = B_0[(\sin \theta \cos \phi)\bar{x} + (\sin \theta \sin \phi)\bar{y} + (\cos \theta)\bar{z}]$ .  $B_0$  corresponds to the Earth's magnetic field,  $\theta$  and  $\phi$  correspond to the orientation of the magnetic field with respect to hyperfine tensor [6],  $J$  and  $D$  are the exchange and dipolar interactions, and  $A$  is the hyperfine tensor depicting interactions between electrons and neighboring nuclear spins.

The spin state of the radical pair evolves under the Zeeman and hyperfine interactions. Along with this evolution, the radical pair also recombines back, as shown in Fig. 1. The recombination either happens back to the ground state or to the signaling state (via protonation with  $H^+$  of the acceptor radical; cf. Fig. 1). The CISS effect plays a role in the formation and recombination of the radical pair as it involves electron transport through the chiral protein molecule. Therefore, the action of CISS is captured by the initial state  $P_I$  and recombination state  $P_R$ , shown with red arrows in Fig. 1. The signaling state does not involve the transfer of electrons (only  $H^+$  involved); therefore, CISS is not involved in its formation (shown with the blue arrow in Fig. 1). We define [20]

$$|\psi_I\rangle = \frac{1}{\sqrt{2}}[\sin(0.5\chi) + \cos(0.5\chi)]|\uparrow_D \downarrow_A\rangle + \frac{1}{\sqrt{2}}[\sin(0.5\chi) - \cos(0.5\chi)]|\downarrow_D \uparrow_A\rangle. \quad (2)$$

Then the initial state density matrix is given as  $P_I = |\psi_I\rangle\langle\psi_I| \otimes \frac{1}{Z}$ , where  $\frac{1}{Z}$  corresponds to the mixed state of the nuclei, and  $Z$  is the size of the nuclear Hilbert space. The recombination operator  $P_R = |\psi_R\rangle\langle\psi_R|$  accounts for recombination to the ground state, where  $|\psi_R\rangle$  is

$$|\psi_R\rangle = -\frac{1}{\sqrt{2}}[\sin(0.5\chi) - \cos(0.5\chi)]|\uparrow_D \downarrow_A\rangle - \frac{1}{\sqrt{2}}[\sin(0.5\chi) + \cos(0.5\chi)]|\downarrow_D \uparrow_A\rangle. \quad (3)$$

The CISS parameter  $\chi \in [0, \frac{\pi}{2}]$  depends on the spin selectivity of the protein medium, with  $\chi = 0$  corresponding to no CISS and  $\chi = \pi/2$  corresponding to the maximum CISS. The master equation governing the state evolution of the system is given as

$$\frac{d\hat{\rho}}{dt} = -i[\hat{H}, \hat{\rho}(t)] - \frac{1}{2}k_R\{P_R, \hat{\rho}(t)\} - k_F\hat{\rho}(t), \quad (4)$$

where  $k_F$  is the protonation rate constant (corresponding to the signaling state) and  $k_R$  is the recombination rate constant (back to the ground state) [20,33].  $[A, B] = AB - BA$  correspond to the commutator, whereas  $\{A, B\} = AB + BA$  is the anticommutator.

## III. RESULTS

This section is divided into three parts. In the first part, we scrutinize the effect of CISS on the local and global coherence measures in the radical-pair mechanism. Interestingly, we observe that the CISS enhances both local and global coherence measures. In the second part, we examine the effect of the dipolar interaction on the global and local coherence measures along with their interplay with the CISS. In the last part, we study the coherence measures in the radical-pair (RP) system as a function of recombination and protonation rate constants ( $k_R$  and  $k_F$ ).

### A. Effect of CISS on quantum coherence measures

To quantify the coherence in the radical-pair system, we use the von Neumann entropy  $S(\rho)$ , given as

$$S(\rho) = -\text{Tr}[\rho \ln(\rho)], \quad (5)$$

where  $\text{Tr}$  represents the trace of a matrix. The von Neumann entropy has a minimum value of zero for pure states and a maximum value of  $\ln(d)$ , where  $d$  is the dimension of the Hilbert space of the system. The maximum value corresponds to the maximally mixed state of the system. With the von Neumann entropy, the coherence quantifier of the RP system can be defined by the relative entropy of local and global coherence, as given in Eq. (6) and Eq. (7), respectively, as [26]

$$C_L(\rho) = S(\rho_{\text{diag}}^{\text{el}}) - S(\rho^{\text{el}}), \quad (6)$$

$$C_G(\rho) = S(\rho_{\text{diag}}) - S(\rho). \quad (7)$$

The relative entropy of local coherence only accounts for the coherence in the electron pair of the radicals, while the relative entropy of global coherence is the measure of the

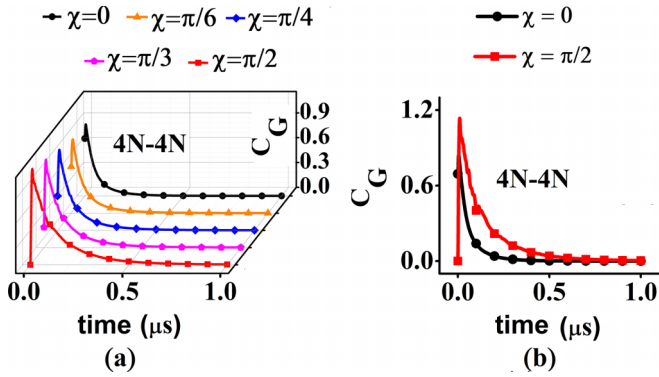


FIG. 2. (a) Relative entropy of global coherence  $C_G$  at  $(k_F, k_R) = (10^6, 10^8) \text{ s}^{-1}$  for five distinct values of  $\chi$  corresponding to varying degrees of spin selectivity due to CISS [0 (black, circle),  $\frac{\pi}{6}$  (orange, triangle),  $\frac{\pi}{4}$  (blue, diamond),  $\frac{\pi}{3}$  (pink, pentagon),  $\frac{\pi}{2}$  (red, square)]. (b) Relative entropy of global coherence  $C_G$  at  $(k_F, k_R) = (10^6, 10^8) \text{ s}^{-1}$  for two extreme cases  $\chi$  [0 (black, circle),  $\frac{\pi}{2}$  (red, square)] showing an increase in coherence time. The calculations have been done for an eight-nuclei (4N-4N) cryptochrome-based radical-pair system with values  $B_0 = 50 \mu\text{T}$ ,  $D = 0$ ,  $J = 0$ ,  $\theta = 0$ ,  $\phi = 0$ .

electron+nuclear system. Therefore, in Eq. (6),  $\rho^{el}$  is the density matrix of the electrons that is obtained after partial trace of  $\rho(t)$  [obtained from Eq. (4)] over the nuclear spin subspace.  $\rho_{\text{diag}}^{el}$  is the density matrix of the electron pair without the off-diagonal terms. In Eq. (7),  $\rho$  is the density matrix of the combined (electrons+nuclei) system, and  $\rho_{\text{diag}}$  is the combined system's density matrix without the off-diagonal terms.  $\rho_{\text{diag}} = \sum_n |n\rangle\langle n| \rho |n\rangle\langle n|$  maps the local( $\rho^{el}$ )/global( $\rho$ ) quantum state into an incoherent state in any basis [10]. We also use a quantifier called the total coherence measure defined in [5] that captures the coherence summed over the entire evolution period. It is given as

$$M_i(\rho) = \int_0^\infty C_i(\rho(t)) dt. \quad (8)$$

Here,  $i \in \{L, G\}$  corresponds to the local and global coherence measures, respectively.

In Fig. 2, we have plotted the relative entropy of global coherence  $C_G(\rho)$  with respect to time at  $\theta = 0$  and  $\phi = 0$ . In Fig. 2(a), we have considered five distinct values of  $\chi$  showing varying degree of spin selectivity due to CISS (0,  $\frac{\pi}{6}$ ,  $\frac{\pi}{4}$ ,  $\frac{\pi}{3}$ ,  $\frac{\pi}{2}$ ). For analysis, we have considered a realistic rate constants combination  $(k_F, k_R) = (10^6, 10^8) \text{ s}^{-1}$  for an eight-nuclei cryptochrome-based radical pair. In Fig. 2(b), we have considered two extreme cases, i.e.,  $\chi = (0, \frac{\pi}{2})$ , highlighting the increase in global coherence measure (magnitude and time duration). A finite value of  $C_G$  for a longer duration of time was observed when  $\chi = \frac{\pi}{2}$  compared to  $\chi = 0$ .

In Fig. 3, we have plotted the relative entropy of local coherence [ $C_L(\rho)$ ] with respect to time. In Fig. 3(a), we consider five distinct values of  $\chi = (0, \frac{\pi}{6}, \frac{\pi}{4}, \frac{\pi}{3}, \frac{\pi}{2})$  for a realistic rate constant of  $(k_F, k_R) = (10^6, 10^8) \text{ s}^{-1}$  for an eight-nuclei cryptochrome-molecule-based radical-pair system. In Fig. 3(b), we have considered two extreme cases, i.e.,  $\chi = (0, \frac{\pi}{2})$ , highlighting the increment in the local coherence measure with CISS. At  $t = 0$ , we observe the maximum value

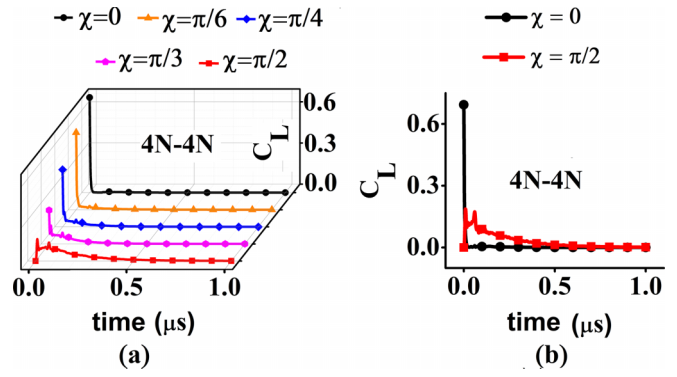


FIG. 3. (a) Relative entropy of local coherence  $C_L$  at  $(k_F, k_R) = (10^6, 10^8) \text{ s}^{-1}$  for five distinct values of  $\chi$  showing varying degree of spin selectivity due to CISS [0 (black, circle),  $\frac{\pi}{6}$  (orange, triangle),  $\frac{\pi}{4}$  (blue, diamond),  $\frac{\pi}{3}$  (pink, pentagon),  $\frac{\pi}{2}$  (red, square)]. (b) Relative entropy of local coherence  $C_L$  at  $(k_F, k_R) = (10^6, 10^8) \text{ s}^{-1}$  for two extreme cases, i.e.,  $\chi = [0$  (black, circle),  $\frac{\pi}{2}$  (red, square)] exhibiting sustained coherence. The calculations have been done for an eight-nuclei (4N-4N) cryptochrome-based radical-pair system with values  $B_0 = 50 \mu\text{T}$ ,  $D = 0$ ,  $J = 0$ ,  $\theta = 0$ ,  $\phi = 0$ .

of  $C_L$  at  $\chi = 0$ . As the CISS parameter ( $\chi$ ) increases,  $C_L$  decreases at  $t = 0$ . It can be attributed to the initial value of  $\rho$  at  $t = 0$ , i.e., as  $\chi$  increases, the nondiagonal elements of the density matrix ( $\rho$ ) associated with radical-pair local coherence decrease. However, even though at  $t = 0$ , the system is showing maximal local coherence ( $C_L$ ) at  $\chi = 0$ , the case of full CISS  $\chi = \frac{\pi}{2}$  shows sustained coherence over the evolution. Hence, we deduce that CISS causes sustained quantum coherence in the radical-pair system.

In our analysis of Figs. 2 and 3, it was observed that an increase in CISS results in an enhancement in quantum coherence measures. We further confirm this by making use of Eq. (8) that captures the coherence over the entire duration of the spin state evolution. We plot  $M_i$  as a function of CISS parameter ( $\chi$ ) in Fig. 4 at realistic rate constants of  $(k_F, k_R) = (10^6, 10^8) \text{ s}^{-1}$  for two-nuclei (black, square), four-nuclei (red, circle), six-nuclei (blue, triangle), and eight-nuclei (pink, pentagon) cryptochrome-based radical-pair systems.

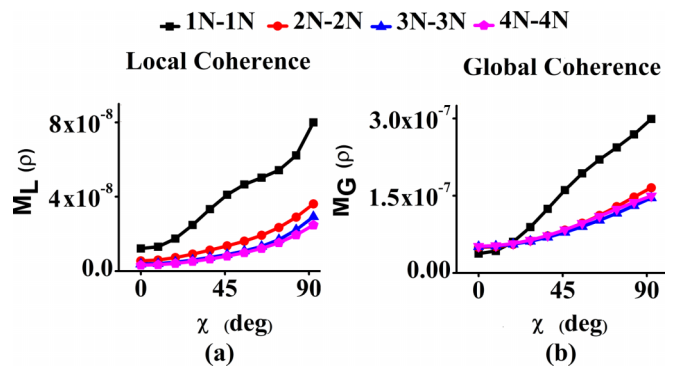


FIG. 4. Relative entropy of (a) local coherence ( $M_L$ ) and (b) global coherence ( $M_G$ ) at  $(k_F, k_R) = (10^6, 10^8) \text{ s}^{-1}$  for  $\chi \in [0, \frac{\pi}{2}]$ . This has been done for two-nuclei (black, square), four-nuclei (red, circle), six-nuclei (blue, triangle), and eight-nuclei (pink, pentagon) cryptochrome-based radical-pair systems. The calculations are done on values  $B_0 = 50 \mu\text{T}$ ,  $D = 0$ ,  $J = 0$ ,  $\theta = 0$ ,  $\phi = 0$ .

TABLE I.  $\Delta M_i$  for radical-pair model based on two, four, six, seven, and eight nuclei from a cryptochrome-based radical-pair system for the rate constant  $(k_F, k_R) = (10^6, 10^8) \text{ s}^{-1}$ .

Nuclei system	$\Delta M_G$	$\Delta M_L$
1N-1N (two-nuclei)	7.97	6.59
2N-2N (four-nuclei)	3.33	6.57
3N-3N (six-nuclei)	2.86	7.83
4N-3N (seven-nuclei)	2.90	7.70
3N-4N (seven-nuclei)	2.88	7.97
4N-4N (eight-nuclei)	2.89	7.74

pentagon) cryptochrome-based radical-pair systems. As is clear from Fig. 4, the total coherence  $M_i$  ( $i \in \{L, G\}$ ) increases with the degree of CISS. As expected, with the inclusion of more nuclei, the total coherence of the system decreases for a fixed value of  $\chi$ . To better analyze this, we define another quantity called  $\Delta M_i$  in Eq. (9) to quantify the change in total coherence  $M_i$  due to CISS,

$$\Delta M_i = \frac{\max_{\chi \in \{0^\circ, 90^\circ\}}(M_i)}{\min_{\chi \in \{0^\circ, 90^\circ\}}(M_i)}. \quad (9)$$

Table I gives the value of  $\Delta M_i$  for these four systems along with two more cases where we have taken seven nuclei (the first case is four on  $\text{FAD}\cdot^-$  and three on  $\text{TrpH}\cdot^+$ ; the second case is three on  $\text{FAD}\cdot^-$  and four on  $\text{TrpH}\cdot^+$ ). We observe that all values are greater than unity, signifying an increase in coherence in all systems. However, the value of  $\Delta M_G$  decreases as the number of nuclei increases up to six and saturates as the number of nuclei are increased above six. In the above analysis, though performed for  $\theta = 0$  and  $\phi = 0$ , the increase in coherence due to CISS was observed at all orientations of the radical with respect to the Earth's magnetic field.

### B. Effect of dipolar interaction

This section examines the effect of spin dipolar interaction along with CISS on coherence in the radical-pair system. Dipolar interaction ( $D$ ) is governed by Eq. (10), where  $r$  is the distance between two electrons [36],

$$D(r) = -\frac{3 \mu_o \gamma_e^2 \hbar^2}{2 4\pi r^3} \Rightarrow D(r)/\mu T = -\frac{2.78 \times 10^3}{(r/nm)^3}. \quad (10)$$

Figure 5 exhibits the effect of dipolar interaction on total global and local coherence measures ( $M_G$  and  $M_L$ ). We plot  $M_G$  [Fig. 5(a)] and  $M_L$  [Fig. 5(b)] with respect to  $\chi$ . We plot for five distinct values of dipolar interaction, assuming there is no exchange interaction for the six nuclei of the cryptochrome molecule. We take realistic values of the rate constant, i.e.,  $(k_F, k_R) = (10^6, 10^8) \text{ s}^{-1}$ , in our analysis.

From both plots in Fig. 5, we observe that the increase in global coherence due to CISS ( $\Delta M_G$ ) remains constant and is unaffected due to dipolar interaction. However,  $\Delta M_L$  is affected by the dipolar interaction and decreases about 13% as  $D$  increases from 0 to 0.4 mT. It is summarized and confirmed in Table II. In Fig. 5(a), we observe that for intermediate values of  $\chi$ , having nonzero dipolar interaction increases the total global coherence. To analyze this further, we define a quantity called  $\Delta G_{D=i}(\chi)$  and  $\Delta L_{D=i}(\chi)$  given in Eq. (11)

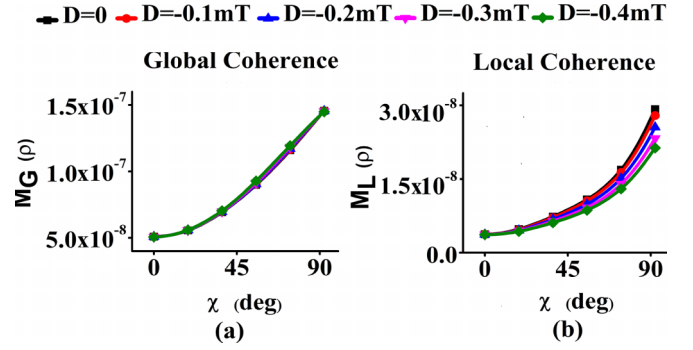


FIG. 5. Relative entropy of (a) global coherence and (b) local coherence at  $(k_F, k_R) = (10^6, 10^8) \text{ s}^{-1}$  for  $\chi \in [0, \frac{\pi}{2}]$ . A total of five values of  $D$  were assumed [0 (black, square), 0.1 mT (red, circle), 0.2 mT (blue, triangle), 0.3 mT (pink, inverted triangle), and 0.4 mT (green, diamond)]. The calculations have been done for six nuclei (3N-3N) from the cryptochrome molecule at  $B_0 = 50 \mu\text{T}$ ,  $J = 0$ ,  $\theta = 0$ ,  $\phi = 0$ .

and Eq. (12), respectively.  $\Delta G_{D=i}(\chi)$  and  $\Delta L_{D=i}(\chi)$  compute the difference of total global (local) coherence when  $D = 0$  and when  $D = i$ , where  $i \in \{0.1 \text{ mT}, 0.2 \text{ mT}, 0.3 \text{ mT}, 0.4 \text{ mT}\}$  at a particular  $\chi$ ,

$$\Delta G_{D=i}(\chi) = M_{G,D=0}(\chi) - M_{G,D=i}(\chi), \quad (11)$$

$$\Delta L_{D=i}(\chi) = M_{L,D=0}(\chi) - M_{L,D=i}(\chi). \quad (12)$$

In Fig. 6, we plot  $\Delta G_{D=i}$  and  $\Delta L_{D=i}$  as function of  $\chi$ . A horizontal reference line in Fig. 6 depicts  $\Delta G_{D=i} = 0$  and  $\Delta L_{D=i} = 0$ . Anything above this line shows that total coherence is greater when  $D = 0$  than  $D = i$ . Figure 6(a) plots  $\Delta G_{D=i}$  where, for intermediate values of  $\chi$ , we observe a negative value of  $\Delta G_{D=i}$ . It signifies that dipolar interaction enhances global coherence for these values of  $\chi$ . The range of values of  $\chi$  for which we observe an increase in coherence is approximately the same for all values of  $D$ . Figure 6(b) discusses  $\Delta L_{D=i}$ , where we observe that  $\Delta L_{D=i}$  is always positive for all values of  $D$ . Hence for all values of dipolar interactions, local coherence shows degradation in total local coherence  $M_L$ . The exchange interaction ( $J$ ) further increases total global coherence, which is discussed in detail in Appendix B.

### C. Coherence in RP mechanism for various rate constant

In this section, we ascertain the enhancement in coherence with CISS at different rate constants. We present Tables III and IV that show an increase in total coherence due to CISS

TABLE II.  $\Delta M_i$  for radical-pair model based on six nuclei (3N-3N) from the cryptochrome molecule for rate constant  $(k_F, k_R) = (10^6, 10^8) \text{ s}^{-1}$ .

Dipolar interaction	$\Delta M_G$	$\Delta M_L$
$D = 0$	2.86	7.82
$D = 0.1 \text{ mT}$	2.86	7.50
$D = 0.2 \text{ mT}$	2.86	6.90
$D = 0.3 \text{ mT}$	2.86	6.31
$D = 0.4 \text{ mT}$	2.86	5.81

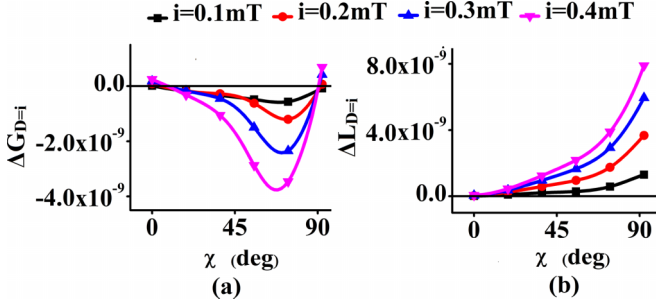


FIG. 6. (a)  $\Delta G_{D=i}$  and (b)  $\Delta L_{D=i}$ , where  $i$  is 0.1 mT (black, square), 0.2 mT (red, circle), 0.3 mT (blue, triangle), and 0.4 mT (pink, inverted triangle) at  $(k_F, k_R) = (10^6, 10^8) \text{ s}^{-1}$  for  $\chi \in [0, \frac{\pi}{2}]$ . The horizontal dotted line is the reference line depicting when  $\Delta G_{D=i} = 0$  and  $\Delta L_{D=i} = 0$ . Anything above this line shows that total coherence is greater for the case when  $D = 0$  than when  $D = i$ . The calculations have been done for six nuclei (3N-3N) from the cryptochrome molecule at  $B_0 = 50 \mu\text{T}$ ,  $J = 0$ ,  $\theta = 0$ ,  $\phi = 0$ .

(through  $\Delta M_G$  and  $\Delta M_L$ ) for a wide range of rate constants. We find that the maximum value of  $\Delta M_G$  is at  $(k_F, k_R) = (10^4, 10^8) \text{ s}^{-1}$  and  $\Delta M_L$  is at  $(k_F, k_R) = (10^4, 10^6) \text{ s}^{-1}$  (i.e., maxima occur at a different rate constant combination). However, interestingly, a lower  $k_F$  (protonation rate constant) is key to achieve a greater increase in coherence due to CISS.

#### IV. EFFECT OF ENVIRONMENTAL DECOHERENCE

In this section, we take into consideration the decoherence effect of the surrounding system. We modify Eq. (4) to add spin decoherence operators in the Lindblad formalism,

$$\begin{aligned} \frac{d\hat{\rho}}{dt} &= -(C + R + D) \\ &= -i[\hat{H}, \hat{\rho}(t)] - \frac{1}{2}k_R\{P_R, \hat{\rho}(t)\} - k_F\hat{\rho}(t) \\ &\quad + k \sum_n \frac{1}{2}\{2C_n\rho(t)C_n^\dagger - \rho(t)C_n^\dagger C_n - C_n^\dagger C_n\rho(t)\}. \end{aligned} \quad (13)$$

In Eq. (13),  $D$  corresponds to the spin decoherence occurring due to the surrounding environment.  $C$  corresponds to the coherent evolution term, and  $R$  corresponds to the recombination term. Mathematically, we take six decoherence operators [6]:  $C_1 = \sigma_x \otimes I_{E_2} \otimes I_N$ ,  $C_2 = \sigma_y \otimes I_{E_2} \otimes I_N$ ,  $C_3 = \sigma_z \otimes I_{E_2} \otimes I_N$ ,  $C_4 = I_{E_1} \otimes \sigma_x \otimes I_N$ ,  $C_5 = I_{E_1} \otimes \sigma_y \otimes I_N$ , and  $C_6 = I_{E_1} \otimes \sigma_z \otimes I_N$ .  $I_{E_1}$  corresponds to the mixed state of

TABLE III.  $\Delta M_G$  for global coherence for radical-pair model based on six nuclei (3N-3N) from the cryptochrome molecule for various rate constant combinations at  $D = 0$  and  $J = 0$ .

$k_R \downarrow, k_F \rightarrow$	$10^4 \text{ s}^{-1}$	$10^5 \text{ s}^{-1}$	$10^6 \text{ s}^{-1}$	$10^7 \text{ s}^{-1}$	$10^8 \text{ s}^{-1}$
$10^4 \text{ s}^{-1}$	0.98	0.87	0.86	0.84	0.68
$10^5 \text{ s}^{-1}$	1.57	0.98	0.86	0.84	0.68
$10^6 \text{ s}^{-1}$	2.44	1.57	0.98	0.86	0.68
$10^7 \text{ s}^{-1}$	2.78	2.50	1.61	0.99	0.71
$10^8 \text{ s}^{-1}$	3.82	3.74	2.86	2.01	0.98

TABLE IV.  $\Delta M_L$  for local coherence for radical-pair model based on six nuclei (3N-3N) from the cryptochrome molecule for various rate constant combinations at  $D = 0$  and  $J = 0$ .

$k_R \downarrow, k_F \rightarrow$	$10^4 \text{ s}^{-1}$	$10^5 \text{ s}^{-1}$	$10^6 \text{ s}^{-1}$	$10^7 \text{ s}^{-1}$	$10^8 \text{ s}^{-1}$
$10^4 \text{ s}^{-1}$	4.53	2.83	2.52	1.51	0.33
$10^5 \text{ s}^{-1}$	13.76	4.52	2.66	1.52	0.33
$10^6 \text{ s}^{-1}$	19.49	13.33	4.13	1.58	0.33
$10^7 \text{ s}^{-1}$	18.56	16.98	10.04	2.10	0.33
$10^8 \text{ s}^{-1}$	9.10	8.82	7.82	2.88	0.37

electron on the  $\text{FAD}^{\cdot-}$  radical, while  $I_{E_2}$  corresponds to the mixed state of electron on the  $\text{TrpH}^{\cdot+}$  radical.  $I_N$  is the combined mixed state of the surrounding nuclei and  $k$  is the decoherence rate constant.

In Fig. 7, we plot total global ( $M_G$ ) and local ( $M_L$ ) coherence as a function of the CISS parameter ( $\chi$ ). This calculation has been done at  $(k_F, k_R) = (10^6, 10^8) \text{ s}^{-1}$  and  $J = 0$  and  $D = 0$ . We observe that at full CISS, both coherence measures achieve maxima even under the effect of environmental decoherence. We have also listed  $\Delta M_G$  and  $\Delta M_L$  with various decoherence rate constant ( $k$ ) values in Table V. We observe a reduction in the value of  $\Delta M_G$  and  $\Delta M_L$  as the decoherence rate constant  $k$  increases. However, interestingly, we observe an increment in coherence due to CISS, even at high decoherence rate values.

#### V. ON CORRELATION OF QUANTUM COHERENCE WITH SIGNALING STATE YIELD

In this section, we correlate coherence measures to the signaling state (forward reaction) yield of the radical-pair reaction (cf. Fig. 1 for signaling state yield), demonstrating the utilitarian role of coherence. We use the correlation coefficient to show a statistical correlation between signaling state yield and the radical-pair spin coherence measures (both local and global). We use numerous orientations of the radical pair with respect to the external magnetic field to show this correlation in a four-nuclei system at  $(k_F, k_R) = (10^6, 10^8) \text{ s}^{-1}$ . The

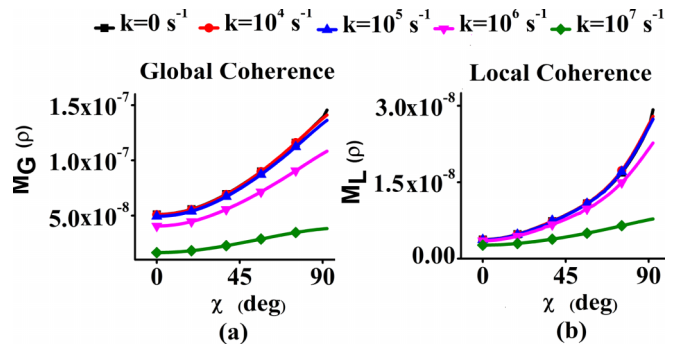


FIG. 7. (a)  $M_G(\chi)$  and (b)  $M_L(\chi)$  where  $k$  is the decoherence rate constant:  $k = 0 \text{ s}^{-1}$  (black, square),  $k = 10^4 \text{ s}^{-1}$  (red, circle),  $k = 10^5 \text{ s}^{-1}$  (blue, triangle),  $k = 10^6 \text{ s}^{-1}$  (pink, inverted triangle), and  $k = 10^7 \text{ s}^{-1}$  (green, diamond). The calculations have been done for six nuclei (3N-3N) from the cryptochrome molecule at  $B_0 = 50 \mu\text{T}$ ,  $J = 0$ ,  $D = 0$ ,  $\theta = 0$ ,  $\phi = 0$ .

TABLE V.  $\Delta M_i$  for radical-pair model based on six nuclei (3N-3N) from the cryptochrome molecule for various relaxation rate constants at  $D = 0$  and  $J = 0$  [ $(k_F, k_R) = (10^6, 10^8) \text{ s}^{-1}$ ].

Relaxation rate constant $k$	$\Delta M_G$	$\Delta M_L$
$k = 0 \text{ s}^{-1}$	2.86	7.82
$k = 10^4 \text{ s}^{-1}$	2.78	7.50
$k = 10^5 \text{ s}^{-1}$	2.76	7.40
$k = 10^6 \text{ s}^{-1}$	2.67	6.44
$k = 10^7 \text{ s}^{-1}$	2.32	2.93

signaling state yield is defined as

$$\phi_F = k_F \int_0^\infty P_S(t) dt = k_F \int_0^\infty \text{Tr}[\rho \hat{\rho}(t)] dt, \quad (14)$$

where  $\rho(\hat{\rho}(t))$  is the solution of the master equation [Eq. (4)],  $\text{Tr}$  is the trace over the state density matrix  $\rho$ , and  $k_F$  is the rate constant associated with the signaling state.

In Fig. 8(a), we have plotted the total global coherence ( $M_G$ ) and the signaling state yield ( $\phi_F$ ) for 2500 combinations of  $\theta$  and  $\phi$ . We have taken the values where  $\theta \in \{0^\circ, 180^\circ\}$  and  $\phi \in \{0^\circ, 360^\circ\}$ . The calculation is performed for no CISS case, i.e.,  $\chi = 0$ . Similarly, in Fig. 8(b), we have plotted the total local coherence ( $M_L$ ) and signaling state yield ( $\phi_F$ ). The  $R$  value (red) corresponds to the correlation coefficient between the coherence measures and signaling state yield. The red line is the linear fit line corresponding to the scattered points. Similar plots have been plotted for the intermediate CISS case (i.e.,  $\chi = \frac{\pi}{4}$ ) in Fig. 9 and the full CISS case (i.e.,  $\chi = \frac{\pi}{2}$ ) in Fig. 10.

The total local coherence measure ( $M_L$ ) has no clear correlation with the signaling state yield ( $\phi_F$ ) for three values of  $\chi$ . The total global coherence ( $M_G$ ) shows a high correlation with the yield of the forward signaling state, i.e., as the degree of CISS increases, the correlation parameter  $R$  between total global coherence and signaling state yield increases. In the full CISS case, the value is near unity, showing a high correlation of global coherence measure with the signaling state yield. The signaling state is thought to be responsible for sending signals to the brain. Hence, global coherence

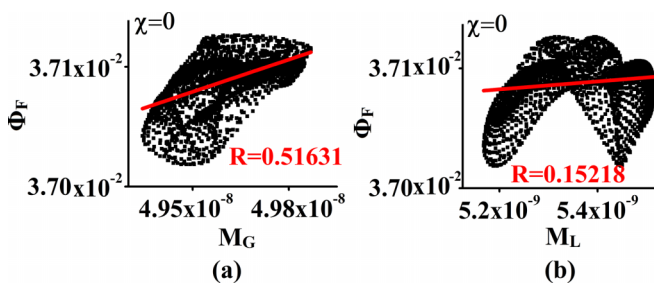


FIG. 8. (a)  $M_G$  vs  $\phi_F$  and (b)  $M_L$  vs  $\phi_F$ , for various values of  $\theta$  and  $\phi$  for  $\chi = 0$ . The calculation is done at  $(k_F, k_R) = (10^6, 10^8) \text{ s}^{-1}$ . The red line corresponds to the linear fit and  $R$  (red) corresponds to the correlation coefficient between the coherence measure and signaling state yield. The calculations have been done for four nuclei (2N-2N) from the cryptochrome molecule at  $B_0 = 50 \text{ } \mu\text{T}$ ,  $J = 0$ ,  $D = 0$ ,  $\theta \in \{0^\circ, 180^\circ\}$ ,  $\phi \in \{0^\circ, 360^\circ\}$ .

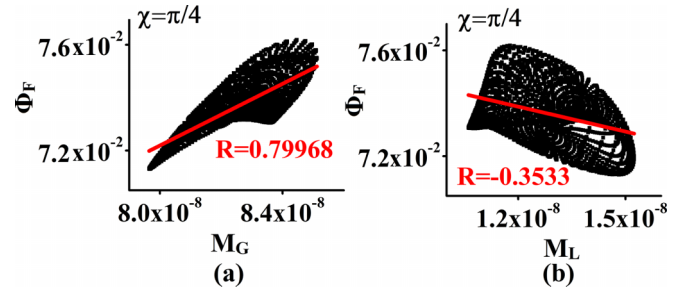


FIG. 9. (a)  $M_G$  vs  $\phi_F$  and (b)  $M_L$  vs  $\phi_F$ , for various values of  $\theta$  and  $\phi$  for  $\chi = \frac{\pi}{4}$ . The calculation is performed at  $(k_F, k_R) = (10^6, 10^8) \text{ s}^{-1}$ . The red line corresponds to the linear fit, and  $R$  (red) corresponds to the correlation coefficient between the coherence measure and signaling state yield. The calculations have been done for four nuclei (2N-2N) from the cryptochrome molecule at  $B_0 = 50 \text{ } \mu\text{T}$ ,  $J = 0$ ,  $D = 0$ ,  $\theta \in \{0^\circ, 180^\circ\}$ ,  $\phi \in \{0^\circ, 360^\circ\}$ .

measures indicate a strong correlation with the later stages of avian magnetoreception. The idea of the utility of global coherence in the radical-pair mechanism (RPM) was first argued in [3] for the RPM where no CISS was considered. In our results, we demonstrate that CISS enhances global coherence, which subsequently would augment the signaling state yield. However, Luo *et al.* [20] have demonstrated that CISS may result in high asymmetric anisotropy of reaction yield that is at odds with behavioral experiments on avian magnetoreception where magnetic field inversion symmetry has been observed [20,37–39]. Therefore, CISS may not be advantageous to the birds for navigation. In addition, an earlier work [33] has shown that another behavioral characteristic of the avian compass, i.e., functional window property, may also not be in consonance with CISS. This leaves us with a broader question about the significance of CISS in radical-pair-based avian navigation. We will leave it to further experiments if the CISS prevails in a realistic cryptochrome-based radical-pair mechanism. That would help in properly assessing the role of CISS in migratory bird navigation.

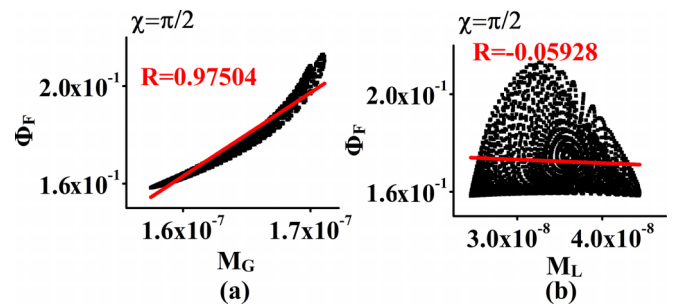


FIG. 10. (a)  $M_G$  vs  $\phi_F$  and (b)  $M_L$  vs  $\phi_F$ , for various values of  $\theta$  and  $\phi$  for  $\chi = \frac{\pi}{2}$ . The calculation is performed at  $(k_F, k_R) = (10^6, 10^8) \text{ s}^{-1}$ . The red line corresponds to the linear fit, and  $R$  (red) corresponds to the correlation coefficient between the coherence measure and signaling state yield. The calculations have been done for four nuclei (2N-2N) from the cryptochrome molecule at  $B_0 = 50 \text{ } \mu\text{T}$ ,  $J = 0$ ,  $D = 0$ ,  $\theta \in \{0^\circ, 180^\circ\}$ ,  $\phi \in \{0^\circ, 360^\circ\}$ .

## VI. CONCLUSION

In conclusion, the chirality-induced spin selectivity (CISS) effect causes quantum coherence to sustain in the radical-pair mechanism. It hints towards the possibility that spin quantum coherence might be sustained in a realistic system despite the presence of multiple nuclei for significant time. Moreover, we also observe that the global coherence in the CISS-assisted avian compass is strongly correlated with the signaling state yield and the correlation increases with the degree of CISS. This indicates that unlike local coherence, global coherence has an important link with the signal going to the avian brain. We also observe that dipolar and exchange interactions are generally detrimental to the quantum coherence in the radical-pair mechanism, but their effect can be countered by the CISS effect. All these conclusions confirm the significance of CISS in the radical-pair mechanism. Interestingly, our results suggest that CISS might help develop quantum technologies (e.g., quantum sensors) where quantum coherence is a resource by sustaining it in engineered systems where a radical-pair-like mechanism is in action. In the future, we plan to harness this aspect of CISS in artificial systems.

## ACKNOWLEDGMENTS

The author would like to thank Aditya Dev (IISER Mohali, India) for insightful discussions. This work is supported by the Science and Engineering Research Board, Department of Science and Technology (DST), India, Grants No. CRG/2021/007060 and No. DST/INSPIRE/04/2018/000023. The authors thank the Department of Electronics and Communication Engineering, IIT Roorkee and the Ministry of Education, Government of India for supporting Y.T.'s graduate research.

## APPENDIX A: HYPERFINE TENSORS

The hyperfine tensors used in our study are based on the work by Hiscock *et al.* [12,13]. The FAD and TrpH molecules are drawn in Fig. 11. The nuclei considered in our simulations on each molecule are marked in red. The hyperfine tensor of all nuclei of the FAD $\cdot^-$  radical considered in our simulations

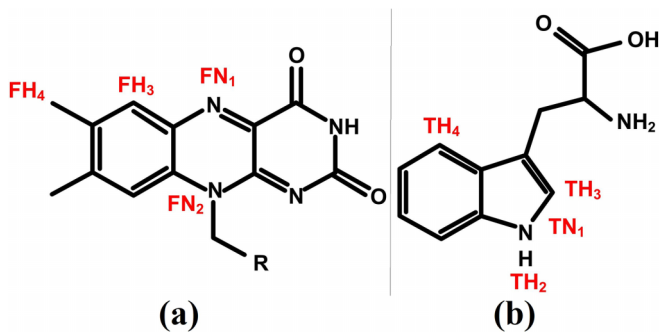


FIG. 11. (a) FAD molecule and (b) TrpH molecule. The nuclei marked in red are considered in our calculation.

is given below:

$$FN_1(mT) = \begin{bmatrix} -0.0989 & 0.0039 & 0 \\ 0.0039 & -0.0881 & 0 \\ 0 & 0 & 1.7569 \end{bmatrix},$$

$$FN_2(mT) = \begin{bmatrix} -0.0190 & -0.0048 & 0 \\ -0.0048 & -0.0196 & 0 \\ 0 & 0 & 0.6046 \end{bmatrix},$$

$$FH_3(mT) = \begin{bmatrix} -0.2569 & -0.1273 & 0 \\ -0.1273 & -0.4711 & 0 \\ 0 & 0 & -0.4336 \end{bmatrix},$$

$$FH_4(mT) = \begin{bmatrix} 0.4399 & 0 & 0 \\ 0 & 0.4399 & 0 \\ 0 & 0 & 0.4399 \end{bmatrix}.$$

The hyperfine tensor of all nuclei of the TrpH $\cdot^+$  radical considered in our simulations is given below:

$$TN_1(mT) = \begin{bmatrix} -0.0336 & 0.0924 & -0.1354 \\ 0.0924 & 0.3303 & -0.5318 \\ -0.1354 & -0.5318 & 0.6680 \end{bmatrix},$$

$$TH_2(mT) = \begin{bmatrix} -0.9920 & -0.2091 & -0.2003 \\ -0.2091 & -0.2631 & 0.2803 \\ -0.2003 & 0.2803 & -0.5398 \end{bmatrix},$$

$$TH_3(mT) = \begin{bmatrix} -0.2843 & 0.1757 & 0.1525 \\ 0.1757 & -0.2798 & 0.0975 \\ 0.1525 & 0.0975 & -0.2699 \end{bmatrix},$$

$$TH_4(mT) = \begin{bmatrix} -0.5596 & -0.1956 & -0.1657 \\ -0.1956 & -0.4020 & 0.0762 \\ -0.1657 & 0.0762 & -0.5021 \end{bmatrix}.$$

## APPENDIX B: EFFECT OF THE EXCHANGE INTERACTION

To understand the dynamics of exchange interaction, we have simulated six-nuclei-based cryptochrome systems. We assume a fixed value of  $D = 0.4$  mT and consider four values of exchange interaction ( $J = 0$ ,  $J = 0.1$  mT,  $J = 0.2$  mT,  $J = 0.3$  mT) [36].

Figure 12(a) exhibits the effect of exchange interaction on total global and local coherence measures ( $M_G$  and  $M_L$ ). We plot  $M_G$  [Fig. 12(a)] and  $M_L$  [Fig. 12(b)] with respect to  $\chi$ . We plot for four distinct values of exchange interaction at  $D = 0.4$  mT for the six nuclei of the cryptochrome molecule. We take realistic values of the rate constants, i.e.,  $[(k_F, k_R) = (10^6, 10^8) \text{ s}^{-1}]$  in our analysis,

$$\Delta G_{J=i}(\chi) = M_{G,J=0}(\chi) - M_{G,J=i}(\chi), \quad (\text{B1})$$

$$\Delta L_{J=i}(\chi) = M_{L,J=0}(\chi) - M_{L,J=i}(\chi). \quad (\text{B2})$$

The increase in global and local coherence for  $D = 0.4$  mT and various  $J$  values are shown in Table VI. In Figs. 12(c) and 12(d), we plot  $\Delta G_{J=i}$  and  $\Delta L_{J=i}$  as a function of  $\chi$ ,

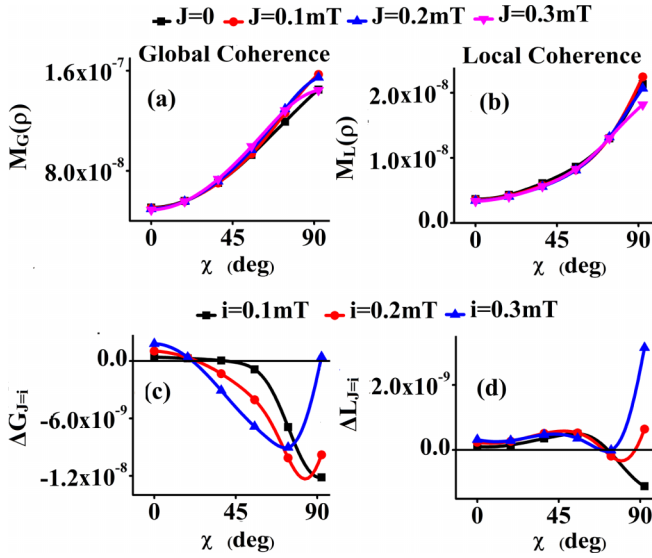


FIG. 12. Relative entropy of (a)  $M_G$  and (b)  $M_L$  at  $(k_F, k_R) = (10^6, 10^8) \text{ s}^{-1}$  for  $\chi \in [0, \frac{\pi}{2}]$ . A total of four values of  $J$  was assumed [0 (black, square), 0.1 mT (red, circle), 0.2 mT (blue, triangle), and 0.3 mT (pink, inverted triangle)]. (c)  $\Delta G_{J=i}$  and (d)  $\Delta L_{J=i}$ , where  $i$  is 0.1 mT (black, square), 0.2 mT (red, circle), and 0.3 mT (blue, triangle) at  $(k_F, k_R) = (10^6, 10^8) \text{ s}^{-1}$ . The horizontal dotted line is the reference line depicting when  $\Delta G_{J=i} = 0$  and  $\Delta L_{J=i} = 0$ . The analysis has been done for six nuclei (3N-3N) at  $B_0 = 50 \mu\text{T}$ ,  $\theta = 0$ ,  $\phi = 0$ , and  $D = 0.4 \text{ mT}$ .

respectively. A horizontal reference line in Figs. 12(c) and 12(d) depicts  $\Delta G_{J=i} = 0$  and  $\Delta L_{J=i} = 0$ . Anything above this line shows that total coherence is greater when  $J = 0$  than  $J = i$ . Figure 12(c) plots  $\Delta G_{J=i}$  where, for intermediate values of  $\chi$ , we observe a negative value of  $\Delta G_{J=i}$ . It signifies that exchange interaction enhances global coherence for these values of  $\chi$ . The range of values of  $\chi$  for which  $\Delta G_{J=i}$  is negative increases with  $J$ . Figure 12(d) discusses  $\Delta L_{J=i}$ , where we observe that  $\Delta L_{J=i}$  is always positive for  $\chi \leq 60^\circ$ . Hence, for  $\chi \leq 60^\circ$ , exchange interactions show degradation in total local coherence  $M_L$ .

### APPENDIX C: PARAMETER INFORMATION

This Appendix summarizes the number of nuclei used for calculation in each figure. This is represented in Table VII. The hyperfine values of each nucleus are given in Appendix A. In Table VIII, we summarize the values of  $\theta$ ,  $\phi$ ,  $D$ ,  $J$ ,  $B_0$  corresponding to each figure. The alphabet  $V$  means that the quantity has multiple (variable) values in that figure.

TABLE VI.  $\Delta M_i$  for radical-pair model based on six nuclei from the cryptochrome molecule for the rate at  $D = 0.4 \text{ mT}$ ,  $(k_F, k_R) = (10^6, 10^8) \text{ s}^{-1}$ .

Exchange interaction	$\Delta M_G$	$\Delta M_L$
$J = 0$	2.86	5.81
$J = 0.1 \text{ mT}$	3.12	6.29
$J = 0.2 \text{ mT}$	3.11	6.03
$J = 0.3 \text{ mT}$	2.95	5.42

TABLE VII. Table depicting information on the number of nuclei considered in each system. The (i) 4N-4N systems have  $FN_1, FN_2, FH_3, FH_4, TN_1, TH_2, TH_3, TH_4$ , (ii) 3N-3N systems have  $FN_1, FN_2, FH_3, TN_1, TH_2, TH_3$ , (iii) 2N-2N systems have  $FN_1, FN_2, TN_1, TH_2$ , and (iv) 1N-1N systems have  $FN_1, TN_1$ . The ‘‘All Comb.’’ used cases of 4N-4N, 3N-3N, 2N-2N, and 1N-1N. The hyperfine tensor  $A$  of each nuclei is given in Appendix A.

Figure	No. nuclei (FAD $\cdot^-$ nuclei - TrpH $\cdot^+$ nuclei)
2	4N-4N (eight nuclei)
3	4N-4N (eight nuclei)
4	All Comb.
5	3N-3N (six nuclei)
6	3N-3N (six nuclei)
7	3N-3N (six nuclei)
8	2N-2N (four nuclei)
9	2N-2N (four nuclei)
10	2N-2N (four nuclei)
12	3N-3N (six nuclei)

TABLE VIII. Table depicting values of the relevant parameters for each figure.  $V$  depicts where the figure has the variable value of that parameter.

Figure	Parameter values
2	$D = 0, J = 0, B_0 = 50 \mu\text{T}, \theta = 0, \phi = 0$
3	$D = 0, J = 0, B_0 = 50 \mu\text{T}, \theta = 0, \phi = 0$
4	$D = 0, J = 0, B_0 = 50 \mu\text{T}, \theta = 0, \phi = 0$
5	$D = V, J = 0, B_0 = 50 \mu\text{T}, \theta = 0, \phi = 0$
6	$D = V, J = 0, B_0 = 50 \mu\text{T}, \theta = 0, \phi = 0$
7	$D = 0, J = 0, B_0 = 50 \mu\text{T}, \theta = 0, \phi = 0$
8	$D = 0, J = 0, B_0 = 50 \mu\text{T}, \theta \in \{0^\circ, 180^\circ\}, \phi \in \{0^\circ, 360^\circ\}$
9	$D = 0, J = 0, B_0 = 50 \mu\text{T}, \theta \in \{0^\circ, 180^\circ\}, \phi \in \{0^\circ, 360^\circ\}$
10	$D = 0, J = 0, B_0 = 50 \mu\text{T}, \theta \in \{0^\circ, 180^\circ\}, \phi \in \{0^\circ, 360^\circ\}$
12	$D = 0.4 \text{ mT}, J = V, B_0 = 50 \mu\text{T}, \theta = 0, \phi = 0$

- [1] A. Chin, S. F. Huelga, and M. B. Plenio, Coherence and decoherence in biological systems: Principles of noise-assisted transport and the origin of long-lived coherences, *Philos. Trans. R. Soc. A* **370**, 3638 (2012).
- [2] V. Salari, J. Tuszyński, M. Rahnama, and G. Bernroider, Plausibility of quantum coherent states in biological systems, *J. Phys.: Conf. Ser.* **306**, 012075 (2011).

- [3] J. Cai and M. B. Plenio, Chemical Compass Model for Avian Magnetoreception as a Quantum Coherent Device, *Phys. Rev. Lett.* **111**, 230503 (2013).
- [4] I. K. Kominis, Quantum relative entropy shows singlet-triplet coherence is a resource in the radical-pair mechanism of biological magnetic sensing, *Phys. Rev. Res.* **2**, 023206 (2020).



- [5] R. Jain, V. S. Poonia, K. Saha, D. Saha, and S. Ganguly, The avian compass can be sensitive even without sustained electron spin coherence, *Proc. R. Soc. A* **477**, 20200778 (2021).
- [6] E. M. Gauger, E. Rieper, J. J. L. Morton, S. C. Benjamin, and V. Vedral, Sustained Quantum Coherence and Entanglement in the Avian Compass, *Phys. Rev. Lett.* **106**, 040503 (2011).
- [7] T. Ritz, S. Adem, and K. Schulten, A model for photoreceptor-based magnetoreception in birds, *Biophys. J.* **78**, 707 (2000).
- [8] V. S. Poonia, D. Saha, and S. Ganguly, State transitions and decoherence in the avian compass, *Phys. Rev. E* **91**, 052709 (2015).
- [9] V. S. Poonia, K. Kondabagil, D. Saha, and S. Ganguly, Functional window of the avian compass, *Phys. Rev. E* **95**, 052417 (2017).
- [10] L. D. Smith, J. Deviers, and D. R. Kattnig, Observations about utilitarian coherence in the avian compass, *Sci. Rep.* **12**, 6011 (2022).
- [11] Y. Zhang, Z. Hu, Y. Wang, and S. Kais, Quantum simulation of the radical pair dynamics of the avian compass, *J. Phys. Chem. Lett.* **14**, 832 (2023).
- [12] H. Hiscock, Long-lived spin coherence in radical pair compass magnetoreception, Ph.D. thesis, University of Oxford, 2018.
- [13] H. G. Hiscock, S. Worster, D. R. Kattnig, C. Steers, Y. Jin, D. E. Manolopoulos, H. Mouritsen, and P. Hore, The quantum needle of the avian magnetic compass, *Proc. Natl. Acad. Sci.* **113**, 4634 (2016).
- [14] R. Naaman and D. H. Waldeck, Chiral-induced spin selectivity effect, *J. Phys. Chem. Lett.* **3**, 2178 (2012).
- [15] R. Naaman and D. H. Waldeck, Spintronics and chirality: Spin selectivity in electron transport through chiral molecules, *Annu. Rev. Phys. Chem.* **66**, 263 (2015).
- [16] C.-H. Ko, Q. Zhu, F. Tassinari, G. Bullard, P. Zhang, D. N. Beratan, R. Naaman, and M. J. Therien, Twisted molecular wires polarize spin currents at room temperature, *Proc. Natl. Acad. Sci.* **119**, e2116180119 (2022).
- [17] S. Ghosh, K. Banerjee-Ghosh, D. Levy, D. Scheerer, I. Riven, J. Shin, H. B. Gray, R. Naaman, and G. Haran, Control of protein activity by photoinduced spin polarized charge reorganization, *Proc. Natl. Acad. Sci.* **119**, e2204735119 (2022).
- [18] A. K. Mondal, M. D. Preuss, M. L. Sleczkowski, T. K. Das, G. Vantomme, E. Meijer, and R. Naaman, Spin filtering in supramolecular polymers assembled from achiral monomers mediated by chiral solvents, *J. Am. Chem. Soc.* **143**, 7189 (2021).
- [19] T. P. Fay, Chirality-induced spin coherence in electron transfer reactions, *J. Phys. Chem. Lett.* **12**, 1407 (2021).
- [20] J. Luo and P. Hore, Chiral-induced spin selectivity in the formation and recombination of radical pairs: Cryptochrome magnetoreception and EPR detection, *New J. Phys.* **23**, 043032 (2021).
- [21] S. Dalum and P. Hedegård, Theory of chiral induced spin selectivity, *Nano Lett.* **19**, 5253 (2019).
- [22] K. Michaeli and R. Naaman, Origin of spin-dependent tunneling through chiral molecules, *J. Phys. Chem. C* **123**, 17043 (2019).
- [23] S. Matityahu, Y. Utsumi, A. Aharony, O. Entin-Wohlman, and C. A. Balseiro, Spin-dependent transport through a chiral molecule in the presence of spin-orbit interaction and nonunitary effects, *Phys. Rev. B* **93**, 075407 (2016).
- [24] B. Göhler, V. Hamelbeck, T. Markus, M. Kettner, G. Hanne, Z. Vager, R. Naaman, and H. Zacharias, Spin selectivity in electron transmission through self-assembled monolayers of double-stranded DNA, *Science* **331**, 894 (2011).
- [25] Y. Sang, F. Tassinari, K. Santra, W. Zhang, C. Fontanesi, B. P. Bloom, D. H. Waldeck, J. Fransson, and R. Naaman, Chirality enhances oxygen reduction, *Proc. Natl. Acad. Sci.* **119**, e2202650119 (2022).
- [26] T. Baumgratz, M. Cramer, and M. B. Plenio, Quantifying Coherence, *Phys. Rev. Lett.* **113**, 140401 (2014).
- [27] A. Streltsov, G. Adesso, and M. B. Plenio, Colloquium: Quantum coherence as a resource, *Rev. Mod. Phys.* **89**, 041003 (2017).
- [28] A. Winter and D. Yang, Operational Resource Theory of Coherence, *Phys. Rev. Lett.* **116**, 120404 (2016).
- [29] J. A. Pauls, Y. Zhang, G. P. Berman, and S. Kais, Quantum coherence and entanglement in the avian compass, *Phys. Rev. E* **87**, 062704 (2013).
- [30] Y. Zhang, G. P. Berman, and S. Kais, The radical pair mechanism and the avian chemical compass: Quantum coherence and entanglement, *Intl. J. Quantum Chem.* **115**, 1327 (2015).
- [31] G. Katsoprinakis, A. Dellis, and I. Kominis, Coherent triplet excitation suppresses the heading error of the avian compass, *New J. Phys.* **12**, 085016 (2010).
- [32] J. Johansson, P. Nation, and F. Nori, QUTIP 2: A PYTHON framework for the dynamics of open quantum systems, *Comput. Phys. Commun.* **184**, 1234 (2013).
- [33] Y. Tiwari and V. S. Poonia, Role of chiral-induced spin selectivity in the radical pair mechanism of avian magnetoreception, *Phys. Rev. E* **106**, 064409 (2022).
- [34] F. Cintolesi, T. Ritz, C. Kay, C. Timmel, and P. Hore, Anisotropic recombination of an immobilized photoinduced radical pair in a 50- $\mu$ T magnetic field: a model avian photomagnetoceptor, *Chem. Phys.* **294**, 385 (2003).
- [35] T. P. Fay, L. P. Lindoy, D. E. Manolopoulos, and P. Hore, How quantum is radical pair magnetoreception? *Faraday Discuss.* **221**, 77 (2020).
- [36] O. Efimova and P. Hore, Role of exchange and dipolar interactions in the radical pair model of the avian magnetic compass, *Biophys. J.* **94**, 1565 (2008).
- [37] W. Wiltschko and R. Wiltschko, Magnetic compass of European robins, *Science* **176**, 62 (1972).
- [38] R. Wiltschko and W. Wiltschko, Magnetoreception in birds, *J. R. Soc. Interface* **16**, 20190295 (2019).
- [39] H. Mouritsen, Long-distance navigation and magnetoreception in migratory animals, *Nature (London)* **558**, 50 (2018).